

Systematic Evaluation of Bonding Strengths and Fracture Toughnesses of Adhesive Joints

Arun Krishnan and L. Roy Xu

Department of Civil and Environmental Engineering,
Vanderbilt University, Nashville, Tennessee, USA

A systematic experimental investigation to determine the shear, tensile, and fracture properties of adhesive joints with bonded same-materials (polymer-polymer) and bi-materials (metal-polymer) is reported. Full-field optical techniques including photoelasticity and coherent gradient sensing (CGS) are employed to record the stress development and failure in these adhesive joints. Five types of strong and weak adhesives are used in conjunction with five different types of materials [aluminum, steel, polymethylmethacrylate (PMMA), polycarbonate, and Homalite[®]-100] to produce a variety of bonded material systems. Weld-on[®]-10 and a polyester bonding consistently show higher tensile and shear bonding strengths. Bi-material systems in shear and fracture report lower properties than the same-material systems due to a higher property mismatch in the former. The resulting complete experimental data are expected to be immensely helpful to computational mechanists in simulating failure mechanics of adhesive joints.

Keywords: Adhesive bonding; Bi-materials; Fracture toughness; Shear strength; Tensile strength

1. INTRODUCTION

A dissimilar-material joint is a special type of material boundary at which two or more different materials are joined together (e.g., aluminum with polycarbonate) by means of an adhesive. This type of an interface poses challenging problems in characterizing its associated

Received 15 November 2009; in final form 14 September 2010.

One of a Collection of papers honoring David A. Dillard, the recipient in February, 2010 of *The Adhesion Society Award for Excellence in Adhesion Science, Sponsored by 3M*.

Address correspondence to L. Roy Xu, Mechanical Engineering Department, University of Texas, 500 W. University Ave., El Paso, TX 79968, USA. E-mail: lrxu@utep.edu

mechanical properties, especially if the constituent materials have a significantly high property mismatch. Dissimilar-material joints have found several engineering applications. Examples include adhesively bonded composite and metal joints in advanced aircraft and ship structures, fiber/matrix interfaces in composite materials, and thin film/substrate structure in micro-electromechanical systems (MEMS), among others. A variety of studies have indicated that failure often occurs along the interface between two different materials with high property mismatch (*e.g.*, free-edge delamination in composite laminates, debonding between thin films/substrates), and that improving the interfacial mechanical properties (especially reducing the interfacial stress level) can modify overall material/structural behavior [1–7]. However, the interfacial strength measurement of dissimilar-material joints remains a challenge due to the stress singularity problem [8–10], *i.e.*, the theoretical interfacial stress will be infinite at the free-edges. On the other hand, modern numerical tools like the cohesive element method have an urgent need for interfacial strengths and fracture toughnesses as important input data. Hence, it becomes necessary to develop reliable quantitative measurements in order to characterize mechanical properties of dissimilar-material joints.

The primary objective of this paper is to measure complete mechanical properties for polymer and metal combinations with different adhesive bonding. The mechanics of bi-materials is complicated; therefore, same-material adhesive joints without high property mismatch will be used to highlight certain simple mechanics aspects involved in the problem. Additionally, we utilize new joint designs to remove the free-edge stress singularity, thereby providing reasonable tensile bonding strength measurements of dissimilar-material joints. We also present resulting fringe patterns from the coherent gradient sensing (CGS) and photoelasticity experiments [11–12], which aid in validating our finite element model. For the sake of completeness and direct comparison, we include some mechanical property data from our previous measurements of dissimilar-material joint systems.

2. EXPERIMENTAL TECHNIQUE AND PROCEDURES

2.1. Jointed Material Combinations with Strong and Weak Adhesive Bonding

This section describes the preparation of specimens and related experimental procedures. Specimens were made of five different types of materials including aluminum-6061-T4, steel-4341, polycarbonate

(Piedmont Plastics, Franklin, TN, USA), PMMA (Piedmont Plastics), and Homalite[®]-100. While the same-material joint specimens were made of PMMA, Homalite[®], polycarbonate, and aluminum, bi-material specimen pairs included PMMA/aluminum, PMMA/steel, polycarbonate/aluminum, and Homalite[®]/steel. Two major types of adhesives were used as bonding agents in most of the specimens. Loctite[®]-384 (Henkel Corp., Rocky Hill, CT, USA), a type of tough acrylic, was used to provide weak bonding. Weld-on[®] (IPS Corp., Gardena, CA, USA), a mixture of an acrylic resin and methyl methacrylate monomer, was used to provide strong bonding. The strength of the bonding is relative and is mainly determined by the chemical aspects of the adhesives as well as how well they bond with materials. A Homalite[®] polyester resin [99.5%] by wt hardened with methyl ethyl ketone peroxide (0.4%) and cobalt octoate (0.1%) as a catalyst (polyester), Loctite 5083, and Loctite 330 were also used as adhesives for interfacial bonding. All these adhesives were specifically chosen because their Young's modulus when cured is close to that of PMMA, polycarbonate, and Homalite[®] (around 2–4 GPa). This ensures that the mechanics of metal/adhesive/polymer joints remains a bi-material mechanics problem and does not become a complicated case involving three different kinds of materials. Every specimen was bonded together from separate halves to enable an interfacial failure and all of the individual bonding surfaces were sandblasted prior to bonding in order to improve the bonding quality. The material used for sandblasting was glass with size of grit #8 (US Filter Inc., Warrendale, PA, USA) at a pressure of 60 psi (0.4 MPa). The bonding itself was enabled by a special fixture to guarantee dimensionality. The specimens were cured for a period of 24 hours in order to achieve the bonding strength under room temperature so the residual stress was almost zero. The thickness of the adhesive layer was less than 20 μm .

2.2. Two Optical Techniques and Experimental Procedures

In order to record *in-situ* fringe patterns developed during the loading process, a mechanical-optical system as illustrated in Fig. 1 was used. This setup included an optical system, a mechanical testing system, and an imaging system. The mechanical testing system consisted of a MTS 810 test machine (MTS Systems Corporation, Eden Prairie, MN, USA) and a loading fixture. The optical system was utilized to capture the *in-situ* fringe pattern development during tests. A laser beam was transmitted through the transparent polymer specimens, and the resulting fringe patterns were recorded by a digital camera.

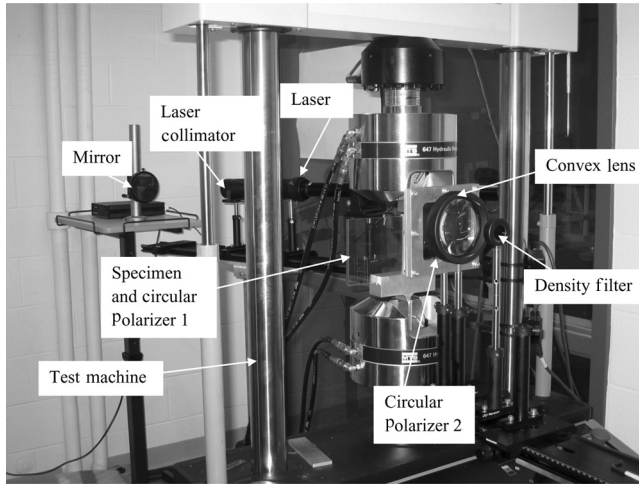


FIGURE 1 Experimental setup of a mechanical-optical system to record in-situ photoelasticity during loading process.

The isochromatic fringe patterns observed in polycarbonate and Homalite[®] specimens are the contours of the maximum in-plane shear stress,

$$\tau_{\max} = \frac{(\sigma_1 - \sigma_2)}{2} = \frac{Nf_{\sigma}}{2h}, \quad (1)$$

where σ_1 and σ_2 are in-plane principal stresses, N is the fringe order, f_{σ} is the stress-fringe constant, and h is the specimen thickness [13]. The optical system included a He-Ne laser source (17 mW), a laser collimator, and a reflection mirror. The collimator was used to provide a large and collimated laser beam of approximately 50-mm diameter. The purpose of the mirror was to adjust the laser beam to a desired position for a specific experiment. The imaging system included a digital camera used to capture fringe development and a density filter in front of the camera to reduce the intensity of the laser beam entering the camera directly. A convex lens with a focal length 150 mm was added to the system to record the whole field of view. An important issue in obtaining good-quality images is to focus the digital camera at infinity, and to ensure that the distance between the convex lens and the specimen is slightly larger than the focal length of the convex lens. Another technique used in this study, coherent gradient sensing technique developed by Tippur et al. [14], was used to obtain fringes of gradients of $\sigma_1 + \sigma_2$ in PMMA specimens, as seen in Fig. 2. Both of these

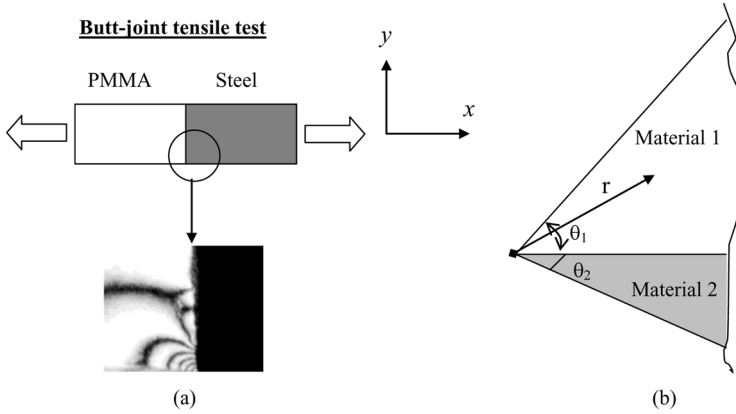


FIGURE 2 (a) Coherent Gradient Sensing (CGS) photograph showing a strong stress concentration (associated with fringe pattern concentrations) at the free edges of a bonded metal and polymer subjected to tensile load (b) Angular definition of a bi-material wedge.

techniques were used to determine the stress state and to observe the crack initiation in our shear specimens.

3. TENSILE STRENGTHS OF SAME AND DISSIMILAR-MATERIAL JOINTS

3.1. Free-Edge Stress Singularity and Specimen Designs to Remove the Stress Singularity

For some specific bi-material corners or edges, several researchers including [15] and [16] have shown that stress singularities exist. The asymptotic stress field of a bi-material corner can be expressed by

$$\sigma_{ij}(r, \theta) = \sum_{k=0}^N r^{-\lambda_k} K_k f_{ijk}(\theta) \quad (i, j = 1, 2, 3), \quad (2)$$

where $f_{ijk}(\theta)$ is an angular function and K_k is also known as the “stress intensity factor.” The fracture mechanics terminology stress intensity factor is used in interfacial mechanics to characterize a similar stress singularity problem. It should be noticed that for an interfacial fracture problem (assuming initial debonding), the stress singularity at a crack tip is intrinsic and cannot be removed. However, the stress singularity in interfacial strength investigation such as bi-material joints (assuming perfect bonding) can be removed through appropriate

designs. The stress singularity order, λ , may be real or complex, and the singularity order is -0.5 for a crack in the same material based on the linear elastic fracture mechanics (LEFM). Hence, the theoretical stress values will become infinite as r (defined in Fig. 2b) approaches zero, if λ has a positive real part. This leads to a problem referred to as the “free-edge stress singularity problem.” It is the presence of this stress singularity that leads to erroneous results in current interfacial strength measurements besides being responsible for free-edge debonding or delamination in dissimilar material joints. But, if λ has a non-positive real part, then the stress singularity disappears.

Bogy [16] found that the stress singularity was purely determined by the material property mismatch and two joint angles of the bi-material corner, θ_1, θ_2 (defined in Fig. 2b). Generally, the material property mismatch can be expressed in terms of the Dundurs’ parameters α and β — two non-dimensional parameters computed from elastic constants of two bonded materials [1]:

$$\alpha = \frac{\mu_1 m_2 - \mu_2 m_1}{\mu_1 m_2 + \mu_2 m_1} \quad \beta = \frac{\mu_1(m_2 - 2) - \mu_2(m_1 - 2)}{\mu_1 m_2 + \mu_2 m_1}, \quad (3)$$

where μ_1 is the shear modulus of Material 1, μ_2 is the shear modulus of Material 2, $m = 4(1 - \nu)$ for plane strain, ν is the Poisson’s ratio, and $m = 4/(1 + \nu)$ for generalized plane stress. The stress singularity order is related to material and geometric parameters, and is determined by a characteristic equation of coefficients A (θ_1, θ_2, p) through F (θ_1, θ_2, p):

$$f(\theta_1, \theta_2, \alpha, \beta, p) = A\beta^2 + 2B\alpha\beta + C\alpha^2 + 2D\beta + 2E\alpha + F = 0, \quad (4)$$

where $p = 1 - \lambda$ and A, B, C, D, E, and F are as defined by [16], and are as listed in the Appendix. Therefore, our basic idea is to vary these four independent parameters ($\theta_1, \theta_2, \alpha, \beta$) in order to obtain a negative real part of the stress singularity order, λ . Xu *et al.* [17] chose an interfacial design with two joint angles: $\theta_1 = 65^\circ$ and $\theta_2 = 45^\circ$ and assumed Material 1 to be a typical hard material and Material 2 to be a soft material. Then, there will be no stress singularity for a wide range of current engineering materials (a small deviation of this pair of joint angles will not change the result). This result is applicable to the entire possible range of the two Dundur’s parameters. For this specific pair of joint angles, the stress singularity is limited to a very small zone near $\alpha \cong 1$. These extreme material joint combinations are quite rare in engineering applications since they represent an extremely high mismatch in Young’s moduli.

Planar and axisymmetric bonded specimens (with the same bonding area) were used for testing specimens in tension. The planar tension specimens are 254 mm long (individual halves are 127 mm long), 38 mm wide, and 6 mm thick. These specimens were used to make same and bi-material joints. The length and thickness of all the specimens were chosen such that the gripping pressure from the MTS system did not cause any specimen damage. The two types of planar tension specimens with straight edges and convex edges are illustrated in Fig. 3a and b, and the two types of axisymmetric specimens with straight edges and convex edges are shown in Fig. 3c and d. The free-edge stress singularity was completely removed in axisymmetric convex joint specimens [18]. In all our reported data of the tensile strengths of bi-material specimens, only axisymmetric specimens with convex edges (Fig. 3d) were used. All of the failure modes were visually observed to be adhesive failure, *i.e.*, failure was always along the interface or bonding line.

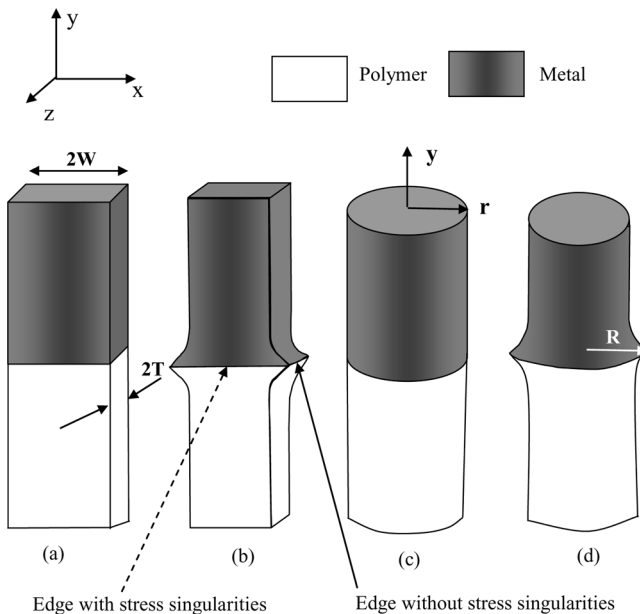


FIGURE 3 Schematic diagrams of metal-polymer joint specimens with (a) straight edges (baseline); (b) convex edges with least stress singularities; (c) axisymmetric straight joints (baseline); (d) axisymmetric convex joints with least stress singularities.

3.2. Comparisons of Tensile Bonding Strengths for Different Material Systems and Adhesives

In each of the tables, such as Table 1, the results for same-material joints are reported first followed by the bi-material data. The first column mentions the type of bonding and the joint materials. The second column presents the data as a mean strength, while the third column reports the difference between the weak and strong bonding of the same-material joints. In all the tables, Loctite adhesives are referred to by their corresponding numbers. For example, 384 would denote the weak bond produced by utilizing Loctite 384 adhesive. W10 refers to the strong adhesive Weld-on[®] 10. This convention is used in all the tables presented in this study.

Material systems bonded with Weld-on[®] 10 show a higher tensile strength, than the same-material systems bonded with Loctite 384 as seen in Table 1. A general trend observed in our tensile strength data is that PMMA material systems show a higher value of tensile strength than polycarbonate systems. All of the specimens were observed to fail in sudden and brittle tension along the interface. To ensure repeatability, at least five specimens were tested in each case. In order to provide a complete database of the same-material bonding of different polymer systems, some results from our previous

TABLE 1 Tensile Bonding Strengths for Same and Bi-Material Joints

Material/adhesive/material	Tensile strength (MPa)	Notes
Same-material bond		
Polycarbonate/384/Polycarbonate	6.06	+113% increase
Polycarbonate/W10/Polycarbonate	12.93	strong/weak
PMMA/384/PMMA	12.66	+64% increase
PMMA/W10/PMMA	20.87	strong/weak
Homalite [®] /Polyester/Homalite [®]	28	[19]
Homalite [®] /W10/Homalite [®]	7.74	
Homalite [®] /330/Homalite [®]	7.0	
Homalite [®] /384/Homalite [®]	6.75	
Homalite [®] /5083/Homalite [®]	1.53	[19]
Bi-material bond		
Polycarbonate/384/aluminum	9.57	[18]
Polycarbonate/W10/aluminum	11.35	
PMMA/384/aluminum	10.01	[18]
PMMA/W10/ aluminum	12.85	[19]
Homalite [®] /330/steel	5.38	
Homalite [®] /384/steel	3.25	

Note: W10 = Weld-on[®] 10.

conference paper [19] are presented in Table 1 along with latest data. Experimental data from our previous work are accumulated here along with currently measured data for the convenience of modeling and simulation work.

For the Homalite[®]/adhesive/Homalite[®] system, in addition to the strong and weak adhesives (Weld-on[®] 10 and Loctite 384), Polyester was also used in strong bonding. The tensile strength of this bond was the highest as Polyester shares a similar chemical structure with Homalite[®] (the major chemical component of Homalite[®] is polyester). Loctite 330 is another strong adhesive similar to Weld-on[®] 10 and its tensile bonding strengths are quite high. Indeed, the weak adhesive Loctite 384 only provided slightly lower bonding strength than Loctite 330 or Weld-on[®] 10. The weakest adhesive bonding is the one using Loctite 5083 adhesive, since its tensile bonding strength is only 20% of the bonding strength using the strong adhesive Weld-on[®] 10 for the same-bonded materials.

Table 1 shows a slight increase in the tensile bonding strengths of bi-materials for those material systems using the Weld-on[®] 10 adhesive. Data related to bi-material bonding are from our previous measurements [18]. Also, bonding strengths of the polycarbonate/aluminum system are just slightly lower than those of PMMA/aluminum system. However, for the Homalite[®]/steel systems, the bonding strength using Loctite 384 is only 32% of the bonding strength of the PMMA/aluminum system. This is probably due to the possibility that the chemical bonding capability of Loctite 383 with steel/Homalite[®] is not as good as that with aluminum/PMMA.

4. SHEAR STRENGTHS OF SAME AND DISSIMILAR-MATERIAL JOINTS

4.1. Specimens and Test Approaches

Shear bonding strength is a key material property for any adhesive joints of dissimilar materials. Previous researchers [6,20] have shown that shear failure is a dominant interfacial failure mode when layered materials with interfaces were subjected to out-of-plane dynamic loading. Thus, for dissimilar-material joints with interfaces, it becomes very necessary to measure the interfacial shear strength for quality control and failure prevention. In our experiments, we measured the interfacial shear strengths over a range of bonded material systems using two types of shear tests: Iosipescu and short-beam shear tests which show different interfacial shear stress distributions. While the short-beam shear specimen shows a parabolic variation of shear stress across its interface, the Iosipescu specimen demonstrates

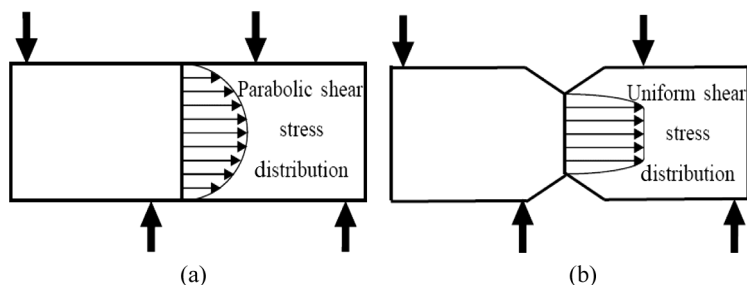


FIGURE 4 Schematic models indicating the structure of (a) Short-beam shear and (b) Iosipescu specimen.

a near constant shear stress variation as illustrated in Fig. 4. The Iosipescu set-up was used to measure the shear strength of both types of specimens with the same specimen width. Iosipescu and short-beam shear specimens were 76.2 mm long (individual halves were 38.1 mm long), 19.1 mm wide, and 5.4 mm thick. In addition, Iosipescu specimens have a notch with a depth of 3.8 mm at the center [21]. Short-beam shear specimens were exclusively utilized to measure the shear strength of the bonded same-materials. Iosipescu shear specimens were used to measure the shear bonding strength for both same-, and bi-material joints.

Coherent gradient sensing experiments were carried out to obtain fringe patterns from bi-material specimens of PMMA/W10/aluminum. This is shown in Fig. 5 where an Iosipescu specimen is subjected to increasing shear load. Aluminum is not transparent and, hence, the fringes were seen only on the PMMA block. The set of four pictures shown in Fig. 5 illustrate the fringe development in the specimen from a small initial load until failure. A strong stress concentration is seen at the loading points and near the concave joint between aluminum and PMMA. Unlike tensile specimens, we were unable to design convex joints for bi-material shear specimens; hence, the free-edge stress singularity still existed in bi-material shear specimens.

In the case of specimens with polycarbonate, photoelasticity experiments were carried out to obtain fringe patterns which are contours of maximum in-plane shear stress given by Eq. (1). These patterns, as seen in Fig. 6, were obtained for short-beam shear specimens at loads of 12.5 and 25% of their final failure load. A finite element model of the specimen was built with ANSYS 11.0 (ANSYS Inc., Canonsburg, PA, USA), to obtain the stress distributions in the bonded specimen. A two-dimensional analysis was employed for bonded polycarbonate

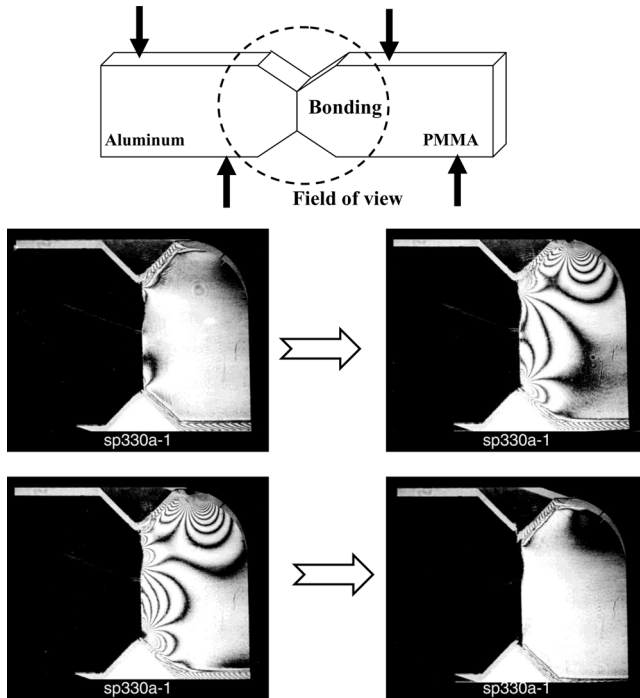


FIGURE 5 CGS fringe pattern development for bonded PMMA/W10/aluminum Iosipescu shear specimen. The first snapshot shows fringe just evolving as the loading is increased and the last snapshot shows the final fracture in the bonded bi-material specimen with a clear shear displacement at the interface.

materials. The mesh was comprised of only Plane 42 elements to meet the requirements of the plotting software Tecplot[®] (Tecplot, Inc., Bellevue, WA, USA). Displacements were applied to the specimen edges to simulate realistic boundary conditions. An iterative procedure was adopted to ensure that the nodes at the lower boundary were free of tensile load as it is impossible for these nodes to be in tension. The obtained loading pattern was anti-symmetric across the interface. Further details of the loading condition and the finite element model can be found in [22]. This stress value was then converted to a fringe, order, N , which, in turn, was converted into a grayscale value. Half-order fringes (0.5, 1.5, 2.5, etc.) were given a value of 255 and full-order fringes (0, 1, 2, etc.) were assigned a value of 0 on the grayscale spectrum. The grayscale values were assigned based on what was observed in the experiments. The half-order fringes are completely

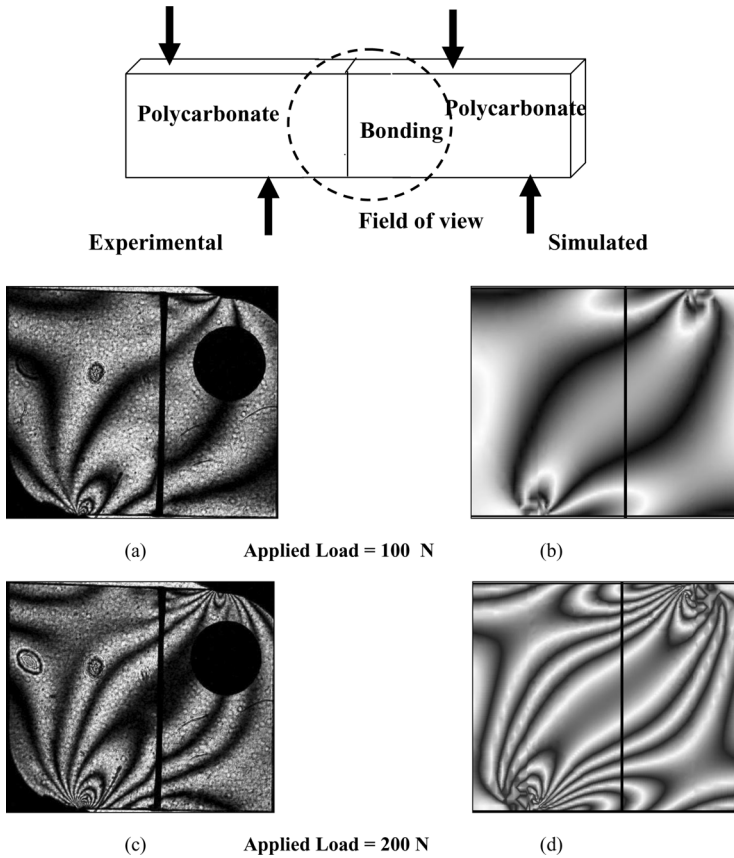


FIGURE 6 Comparison between experimental and finite element generated fringe patterns for a typical polycarbonate short-beam shear specimen.

dark and, hence, have a value of 255, and *vice versa* for the full-order fringes. The resulting fringe patterns, plotted with Tecplot, are compared with the experimentally observed patterns as depicted in Fig. 6. A close match was obtained between the simulated and experimental patterns, thereby validating our finite element model.

4.2. Shear Strength Comparisons and Effect of the Interface Shear Stress on the Bonding Strength

The shear strengths from the different material-systems are reported in Tables 2 and 3. The shear strength values were obtained by using

TABLE 2 Shear Bonding Strengths for Same and Bi-Material Joints

Material/adhesive/material	Shear strength (MPa)	Notes
Same-material bond		
Polycarbonate/384/Polycarbonate	10.99	+41%
Polycarbonate/W10/Polycarbonate	15.52	
PMMA/384/PMMA	11.58	+119%
PMMA/W10/PMMA	25.35	
Homalite [®] /W10/Homalite [®]	>21.65	[19]
Homalite [®] /Polyester/Homalite [®]	>23.26	
Homalite [®] /330/Homalite [®]	12.58	
Homalite [®] /384/Homalite [®]	7.47	
Homalite [®] /5083/Homalite [®]	0.81	[19]
Bi-material bond		
Polycarbonate/384/aluminum	6.18	65%
Polycarbonate/W10/aluminum	10.18	
PMMA/384/aluminum	8.63	18%
PMMA/WD10/aluminum	10.16	

Note: W10 = Weld-on[®] 10.

the failure load divided by cross-sectional area. Table 2 presents shear strength data obtained exclusively by testing Iosipescu shear specimens for a variety of indicated material systems. In each case, about five to six specimens were tested to ensure repeatability and the mean values are reported here. All the shear specimens were found to fail in shear along the bonding line in a sudden and brittle fashion except for Homalite[®]/W10/Homalite[®] and Homalite[®]/polyester/Homalite[®] systems. Bonded same-materials consistently show a greater value of shear strength in comparison with bi-material systems with the same adhesive bonding. This is attributed to a weaker bonding in the case of bi-materials due to high interfacial stress caused by the mismatch in elastic properties. Similar to tensile bonding strengths, material systems with PMMA show a higher value of mean shear strength than systems with polycarbonate. Again, the difference

TABLE 3 Shear Bonding Strengths of Iosipescu and Short-Beam Shear Specimens

Material/adhesive/material	Iosipescu shear (MPa)	Short-beam shear (MPa)	Difference
Aluminum/384/Aluminum	10.75	10.16	5.5%
Polycarbonate/384/Polycarbonate	10.99	8.51	22.5%
PMMA/384/PMMA	11.58	10.19	12%

between Loctite 384 and Weld-on[®] 10 bonding is significantly higher for PMMA-bonded specimens than its polycarbonate counterparts in the case of the same-material bonding. Materials bonded with Weld-on consistently report a value of higher shear strength than Loctite 384.

Bonding strengths of Homalite[®]/adhesive/Homalite[®] systems using different adhesives are also presented in Table 2. Shear bonding strengths of the same-material systems show very different values for various adhesives just as in tensile bonding strengths of the same Homalite[®]/adhesive/Homalite[®] systems. Homalite[®] shear specimens bonded with the strong adhesives Weld-on[®] 10 and polyester were found to fail in tension in the Homalite[®] part, rather than in shear across the bonded interface [23]. Thus, its actual shear bonding strength cannot be measured; but, the lower limit of the shear bonding strength is obtained as seen in Table 2. However, for PMMA and polycarbonate, actual shear bonding strengths can be measured using Iosipescu shear tests as their tensile strengths are much higher than that of Homalite[®].

Table 3 contains shear strength data obtained from both Iosipescu and short-beam shear tests. Here, in each case, about 25–30 specimens were tested. Also, specimens for which data are reported in Table 3 were bonded only using weak adhesive Loctite 384. These data indicate only a small difference between measured shear bonding strengths of Iosipescu and short-beam shear specimens, although their interfacial shear stress distributions are very different, as shown in Fig. 4. Therefore, interfacial shear stress distributions have the least effect on the shear strength measurements for materials with preferred interfaces such as woods and fibrous composites. Obviously, short-beam shear specimens are easier to machine than the Iosipescu shear specimens [22].

5. FRACTURE TOUGHNESS FOR SAME AND DISSIMILAR-MATERIAL JOINTS

5.1. Principles on Fracture Toughness Measurements

Edge-notched fracture specimens were used to measure the Mode-I fracture toughness. The same-material joint specimens were designed and tested to the following dimensions (individual halves): specimen width $W=38$ mm, specimen thickness $B=5.4$ mm, and initial crack length $a=19$ mm. All specimens had an initial crack with $a/W=0.5$ made before bonding by using Scotch[®] tapes. All of the fracture specimens were tested in three-point bending [24]. For bi-material specimens with individual halves having length of 60 mm, width of

$W = 30$ mm, and thickness of $B = 5.4$ mm, their initial crack length, a , was 15 mm, as shown in Fig. 7.

The Mode-I fracture toughness, K_{IC} , for same-material joints was calculated using Eq. (5) [25]:

$$K_{IC} = \left(\frac{P_Q S}{B W^{3/2}} \right) f(x) \quad 0 < x = a/W < 1$$

$$f(x) = \frac{3}{2} \sqrt{x} \frac{[1.99 - x(1-x)(2.15 - 3.93x + 2.7x^2)]}{(1+2x)(1-x)^{3/2}}, \quad (5)$$

where P_Q is the maximum load from the load-displacement plot, S is the support span (here 100 mm), and $f(x)$ accounts for the correction due to the specimen geometry. In the case of bi-materials, the calculation of fracture toughness becomes very different. First, the asymptotic stress field of an interfacial crack in a bi-material specimen, σ_{ij} , can be expressed as [26]

$$\sigma_{ij} = \frac{1}{\sqrt{2\pi r}} [\text{Re}\{K r^{i\epsilon}\} \sigma_{ij}^{-I}(\theta; \epsilon) + \text{Im}\{K r^{i\epsilon}\} \sigma_{ij}^{-II}(\theta; \epsilon)], \quad (6)$$

where $K = K_1 + iK_2$ is the complex stress intensity factor, σ_{ij}^I and σ_{ij}^{II} are the stresses in Mode-I and Mode-II, and ϵ is a function of Dundur's parameters, β , and is given by:

$$\epsilon = \frac{1}{2\pi} \ln \left\{ \frac{1-\beta}{1+\beta} \right\}. \quad (7)$$

The elastic properties of aluminum include a Young's modulus of $E = 71$ GPa, a shear modulus $\mu = 26.7$ GPa, and a Poisson's ratio of $\nu = 0.33$. Corresponding elastic properties for polycarbonate used in this calculation are $E = 2.4$ GPa, $\mu = 0.9$ GPa, and $\nu = 0.34$. Hence,

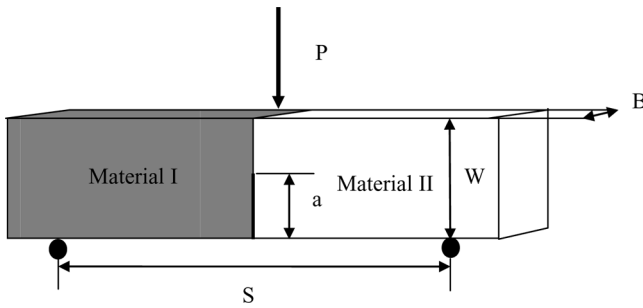


FIGURE 7 Bi-material specimen for mode-I fracture toughness measurement ($a/W = 0.5$).

the two Dundur's parameters for the material combination of polycarbonate and aluminum are calculated as $\alpha = 0.93$ and $\beta = 0.31$. It should be noted here that PMMA, although chemically different, has similar elastic properties similar to polycarbonate. Therefore, the Dundur's parameters for PMMA/aluminum are also close to the values given above. A schematic of our bi-material specimen used to obtain the fracture toughness value is illustrated in Fig. 7.

A general form for the stress intensity factor for a bi-material specimen is given as [27]

$$K = YT\sqrt{a}a^{-i\epsilon}e^{i\psi}, \quad (8)$$

where $T = P(3S/W^2)$ and Y and ψ are calibrating factors which depend on a/W , B/W , and the Dundur's parameters. Then the stress intensity factor in Mode-I can be expressed as

$$K_I = \text{Re}\{Ka^{i\epsilon}\}. \quad (9)$$

Using Eq. (8) and (9), the bi-material fracture toughness, K_{IC} , is calculated as

$$K_{IC} = \frac{3P_Q S}{BW^2} Y \sqrt{a} \cos(\psi) \quad (10)$$

Here, $Y = 2.4$ and $\psi = 7.8$ degrees; the fitting parameters are obtained from [27] for $\beta = \alpha/3$, as is in our case.

5.2. Fracture Toughness Results

The material systems and their measured K_{IC} values are presented in Table 4. During experiments, the load required to break the specimen completely under three-point bending was recorded and the value of K_{IC} was calculated using Eq. (5) for same-material joints and using Eq. (10) for bi-material systems. It was observed that Weld-on[®] 10 bonding shows a higher value of K_{IC} than Loctite 384 bonding for most material systems. There is an increase in K_{IC} of the strong bonding over the weak bonding by 36% for the same-material specimens, and by 85% for bi-material specimens with polycarbonate involved. Similar to its tensile and shear bonding strengths, PMMA shows a better bonding with the two types of adhesives and, hence, a greater value of fracture toughness is obtained for bonded PMMA specimens than for bonded polycarbonate specimens. Meanwhile, bi-material specimens consistently show a lower value of Mode-I fracture toughness than the corresponding same-material specimens.

TABLE 4 Mode-I Fracture Toughness for Same and Bi-Material Joints

Material/adhesive/material	Mean K_{IC} (MPa m ^{1/2})	Difference (%)
Same-material bond		
Polycarbonate/384/Polycarbonate	0.64	+36%
Polycarbonate/W10/Polycarbonate	0.86	
PMMA/384/PMMA	0.71	+147%
PMMA/W10/PMMA	1.74	
Homalite [®] /Polyester/Homalite [®]	0.56	[19]
Homalite [®] /W10/Homalite [®]	0.83	
Homalite [®] /330/Homalite [®]	0.75	
Homalite [®] /384/Homalite [®]	0.38	
Homalite [®] /5083/Homalite [®]	0.19	[19]
Bi-material bond		
Polycarbonate/384/Aluminum	0.13	+85%
Polycarbonate/W10/Aluminum	0.24	
PMMA/384/Aluminum	0.15	+87%
PMMA/W10/Aluminum	0.28	

Surprisingly, Homalite[®]/polyester/Homalite[®] material systems show lower fracture toughness than other strong adhesive systems used in conjunction with Homalite[®]: Weld-on[®] 10 and Loctite 330. It should be noted that polyester provides the highest tensile and shear bonding strengths, as can be seen in Tables 1 and 2. Therefore, strength and fracture toughness are very different parameters and should be measured for every new material system. The fracture toughnesses of other adhesive systems show a trend similar to the bonding strengths of the same- material joints, *i.e.*, bonding strengths increase with fracture toughnesses from weak bonding to strong bonding.

6. CONCLUSIONS

Five different types of strong and weak adhesives (Weld-on[®] 10, Loctite 384, Loctite 330, Loctite 5083, and a polyester) were used in conjunction with five types of materials (aluminum, steel, PMMA, polycarbonate, and Homalite[®]) to produce a variety of bonded material systems. These material systems (same- and bi-material joints) were tested in shear, tension, and fracture. Results indicate that materials bonded with Weld-on[®] 10 and polyester consistently show higher tensile and shear bonding strengths than the same-material systems bonded with other adhesives. In general, bi-material systems in shear and fracture show lower properties than the same-material systems due to higher property mismatch involved in bi-material systems. Specimens bonded with PMMA consistently

show higher values of shear and tensile bonding strengths, and Mode I fracture toughness, than polycarbonate systems. On the significance of the present investigation, a wide variety of carefully measured experimental data will be very beneficial for computational simulations on failure mechanics of adhesive joints.

ACKNOWLEDGMENTS

The authors acknowledge the support from the Office of Naval Research (Program manager Dr. Yapa D.S. Rajapakse) and the National Science Foundation.

REFERENCES

- [1] Hutchinson, J. W. and Suo, Z., *Adv. Appl. Mech.* **29**, 63–191 (1992).
- [2] Gupta, V., Yuan, J., and Pronin, A., *J. Adhes. Sci. Tech.* **8**, 713–747 (1994).
- [3] Lara-Curzio, E., Ferber, M. K., Besmann, T. M., Rebillat, F., and Lamon, J., *Ceram. Engng. Sci.* **15**, 597–612 (1995).
- [4] Needleman, A. and Rosakis, A. J., *J. Mech. Phys. Solids* **47**, 2411–2449 (1999).
- [5] Martin, E., Leguillon, D., and Lacroix, C., *Compos. Sci. Technol.* **6**, 1671–1679 (2001).
- [6] Xu, L. R. and Rosakis, A. J., *Int. J. Solids Struct.* **39**, 4237–4248 (2002).
- [7] Wang, J., *Exp. Mech.* **22**, 249–257 (2007).
- [8] Reedy, ED Jr. and Guess, T. R., *Int. J. Solids Struct.* **30**, 2929–2936 (1993).
- [9] Akisanya, A. R. and Fleck, N. A., *Int. J. Solids Struct.* **34**, 1645–1665 (1997).
- [10] Tandon, G. P., Kim, R. Y., Warrier, S. G., and Majumdar, B. S., *Composites, Part B* **30**, 115–134 (1999).
- [11] Singh, R. P., Lambros, J., Shukla, A., and Rosakis, A. J., *Proc. R. Soc. London, Ser. A* **453**, 2649–2667 (1997).
- [12] Xu, L. R. and Rosakis, A. J., *Opt. Laser Engng.* **40**, 263–288 (2003).
- [13] Kobayashi, A.S. (Ed.), *Handbook on Experimental Mechanics* (Society for Experimental Mechanics, Inc., Prentice-Hall, New Jersey, 1987).
- [14] Tippur, H.V., Krishnaswamy, S., and Rosakis, A.J., *Int. J. Fract.* **48**, 193–204 (1991).
- [15] Williams, M. L., *J. Appl. Mech.* **19**, 526–528 (1952).
- [16] Bogy, D. B., *J. Appl. Mech.* **38**, 377–386 (1971).
- [17] Xu, L. R., Kuai, H., and Sengupta, S., *Exp. Mech.* **44** (6), 608–615 (2004a).
- [18] Wang, P. and Xu, L. R., *Mech. Mater.* **38**, 1001–1011 (2006).
- [19] Xu, L. R., Samudrala, O., and Rosakis, A. J., *Proceedings of the 2002 SEM Annual Conference and Exposition on Experimental and Applied Mechanics* (Paper 34 Society for Experimental Mechanics, Inc., Bethel, CT, USA, 2002).
- [20] Kitey, R. and Tippur, H., *Exp. Mech.* **48**, 37–54 (2008).
- [21] Deng, S., Qi, B., Hou, M., Ye, L., and Magniez, K., *Composites, Part A* **40**, 1698–1707 (2009).
- [22] Krishnan, A. and Xu, L. R., *Exp. Mech.* **50**, 283–288 (2010).
- [23] Xu, L. R., Sengupta, S., and Kuai, H., *Int. J. Adhes. Adhes.* **24**, 455–460 (2004b).
- [24] Suresh, S., Shih, C. F., Morrone, A., and O'Dowd, N. P., *J. Am. Ceram. Soc.* **73** (5), 1257–1267 (1990).

- [25] Anderson, T. L., *Fracture Mechanics*, 2nd ed. (CRC Press, Boca Raton, 1995).
 [26] Rice, J. R., *J. Appl. Mech.* **55**, 98–103 (1988).
 [27] O'Dowd, N. P., Shih, C. F., and Stout, M. G., *Int. J. Solids Struct.* **29** (5), 571–589 (1992).

APPENDIX

A, B, C, D, E, and F are expressed as follows [16]:

$$\begin{aligned}
 A(\theta_1, \theta_2, p) &= 4K(p, \theta_1)K(p, \theta_2), \\
 B(\theta_1, \theta_2, p) &= 2p^2 \sin^2(\theta_1)K(p, \theta_2) + 2p^2 \sin^2(\theta_2)K(p, \theta_1), \\
 C(\theta_1, \theta_2, p) &= 4p^2(p^2 - 1)\sin^2(\theta_1)\sin^2(\theta_2) + K[p, (\theta_1 - \theta_2)], \\
 D(\theta_1, \theta_2, p) &= 2p^2[\sin^2(\theta_1)\sin^2(p\theta_2) - \sin^2(\theta_2)\sin^2(p\theta_1)], \\
 E(\theta_1, \theta_2, p) &= -D(\theta_1, \theta_2, p) + K(p, \theta_2) - K(p, \theta_1), \\
 F(\theta_1, \theta_2, p) &= K[p, (\theta_1 + \theta_2)],
 \end{aligned} \tag{A1}$$

Where the auxiliary function $K(p, x)$ is defined by

$$K(p, x) = \sin^2(px) - p^2 \sin^2(x). \tag{A2}$$